Plasmonics
October 2020, Volume 15, Pages 1533-1539
https://doi.org/10.1007/s11468-020-01177-9
https://archimer.ifremer.fr/doc/00628/73962/

Sensing Polymer/Paracetamol Interaction with an Independent Component Analysis-Based SERS-MIP Nanosensor

Decorbie N. [1], Tijunelyte I. [1], Gam-Derouich S. [2], Solard J. [3], Lamouri A. [2], Decorse P. [2], Felidj N. [2], Gauchotte-Lindsay C. [4], Rinnert Emmanuel [5], Mangeney C. [2, 6], Lidgi-Guigui N. [1, *]

[1] CSPBAT, (now LSPM), Sorbonne Paris Nord, 99 Av. JB Clément, 93430, Villetaneuse, France
[2] Univ Paris Diderot, Sorbonne Paris Cité, ITODYS, UMR CNRS 71086, 75013, Paris, France
[3] Centrale de Proximité en Nanotechnologies de Paris Nord, Sorbonne Paris Nord, 99, Av. JB Clément, 93430, Villetaneuse, France
[4] James Watt School of Engineering, University of Glasgow, Rankine Building, Oakfield Avenue, G12 8LT, Glasgow, UK
[5] IFREMER, RDT-LDCM, Technopole Brest-Iroise, 29280, Plouzané, France
[6] University of Paris, Lab Chim & Biochim Pharmacolog & Toxicol, UMR 8601, 75006, Paris, France

* Corresponding author : N. Lidgi-Guigui, email address : nathalie.lidgi-guigui@univ-paris13.fr

Abstract :

In this article, we propose a new strategy to build a sensor for easy handling and rapid analysis on-site. Our sensor is based on the combination of surface-enhanced Raman spectroscopy (SERS) and molecularly imprinted polymers (MIPs). SERS provides a strong sensitivity for the detection of trace molecules while MIPs offer a highly selective and specific recognition platform. The research presented here focuses on the detection of the interaction between a robust ultra-thin layer of MIPs and of paracetamol, the targeted molecule. This drug is an environmental emerging pollutant, i.e., a molecule whose presence and significance have not yet been elucidated, which gives rise to health and environmental concerns. The results are a combined analysis of the SERS spectra and a multivariate analysis. The former provides a clear demonstration of the evolution of the MIP-nanostructure interaction when the concentration of paracetamol increases. The statistical analysis produces the proof of the selectivity of the sensor

1 INTRODUCTION

Molecularly imprinted polymers (MIPs) are highly selective materials made of robust artificial polymer matrices which ensure long-term stability and can compete with biological receptors like aptamers or antibody [1–3]. MIPs are obtained by the synthesis of crosslinked polymers in the presence of a template molecule which, after extraction, leaves complementary cavities in the film. Rebinding the template by the MIPs is highly specific and selective as the artificial receptors are shaped by the template[4]. The main figure of merit of MIPs compare to their biological counterparts include simple synthesis pathway and low cost, high stability to extreme chemical environment and remarkable reusability. They are especially appropriate for the detection of small molecular compounds; this is probably why their occurrence in environmental sciences is increasing (about 10% of the publications of MIPs for sensors according to web of science) [5]. In the framework of sensing, MIPs are used mainly with electrochemical sensors but also with quartz microbalance [6]. While MIP-based sensors are a thriving research field, there are still only limited numbers of studies combining MIPs with plasmonic nanoparticles. In particular, their combination to lithographic nanoparticles has never been reported so far.

We propose here to graft MIPs onto gold nanostructures and to use this hybrid system as an original SERS (Surface-Enhanced Raman Spectroscopy)/MIPs hybrid sensor. SERS combines rich chemical fingerprint information based on Raman spectroscopy and high sensitivity due to the local field enhancement offered by optically resonant metal nanoparticles. This results in a strong amplification of the Raman signals and label-free identification of molecular species with high-sensitivity. Besides, the SERS analysis can be performed in aqueous medium under ambient conditions, which makes it well adapted for analytical chemistry. Considerable progress has been made in this field, from studies of model systems on roughened metallic surfaces, sensing and imaging applications, to single molecule detection [7–13]. However, tremendous challenges remain in terms of reproducibility and sensitivity. To obtain highly sensitive SERS-active substrates, the most common strategies rely on disorganized nanostructures such as plasmonic colloidal films[14], metallic nano-island layers on glass[15–17] or electrochemically roughened metallic surface[18]. While being simple to prepare and highly sensitive, these substrates offer poor reproducibility, originating from the complexity and heterogeneity of these irregular surfaces, which makes quantitative analysis a difficult task. Some strategies are, however, found to build organized nanostructured surfaces, for example by exploiting the organized array of nanorods left by a coffee stain

[19] or using electroplating on top of a lithographied array [20]. To overcome this issue and achieve more uniform SERS signals, plasmonic substrates with controlled nanostructuration were elaborated using Electron Beam Lithography (EBL). This approach provides a precise control over the geometry and separation of nanostructures, guaranteeing a fabrication reproducibility and precision down to the nanometer scale.

The grafting of a probe molecule on a SERS substrate usually rely on thiol-based strategies. They exhibit excellent bonding affinity between sulfur and gold [8,21,22], however, unfavorable reaction conditions may deteriorate their recognition efficiency. Moreover, during the SERS measurement, the excitation of localized surface plasmon resonance may increase the surface temperature, leading to the desorption and photodecomposition of these chemoreceptor layers and of their thiol-metal links[23,24]. This is why we have chosen here to use a more efficient strategy for the grafting of MIPs. Diazonium salt-based MIPs were synthesized to assure a good stability. We present an original hybrid MIP-SERS sensor easy to prepare, low-cost and reusable. Another of its advantage is that its all-solid form and the lack of treatment of the sample is suitable for *in situ* measurements.

Paracetamol was chosen as the target molecule as it is a widely used drug with analgesic and antipyretic properties, considered nowadays as an emerging pharmaceutical contaminant[25,26]. Owing to its intense use, high excretion rate, persistence and resistance to conventional wastewater treatments, it is found widespread in wastewaters, water effluents, and surface waters, in concentrations ranging from $ng.l^{-1}$ to $\mu g.l^{-1}$. The sensitive detection of paracetamol is an important issue for several reasons. For instance, it can be found unmetabolized in urban wastewaters where the measurement of its concentration is fundamental for epidemiology analysis. A mapping of the concentration of paracetamol can be used to study the actual consumption of this drug by a population in a given area, just as it has already been done by the group J. B. Quintana on many molecules [27,28]. Another point is that paracetamol, metabolized or not, can react with chemicals used in wastewater plants such as hypochlorite to form toxic compound [29]. Finally, paracetamol is part of a larger family of similar compound such as its metabolized compounds or even salicylic acid or acetyl salicylic acid. The process developed here stand as a proof of concept for all these molecules.

To go one step further we have used numerical routine to discriminate between the three above molecules. Independent Components Analysis (ICA) was applied as a chemometric tool to analyze the paracetamol spectra. ICA is a statistical and computational technique for extracting source signals from their mixture. We show that it can be used to differentiate the spectra of the polymer with or without the drugs.

2 MATERIAL AND METHODS

2.1 Reagents

Paracetamol, methacrylic acid (MAA) and ethylene glycol dimethacrylate (EGDMA) were purchased from Sigma-Aldrich and used as received. 4-aminobenzophenone was obtained from Alfa Aesar. N,N-dimethyaniline, chloroform ($CHCl_3$), methanol (MeOH), acetonitrile (ACN), dichloromethane (DCM) and acetone were all of analytical reagent grade from Acros Organics. Water was deionized using a Millipore purification system.

2.2 Synthesis of the initiator derived from diazonium salt C_6H_5-CO-C_6H_4-N_2^+,BF_4^-

The initiator derived from diazonium salt was prepared by standard method of Pinson and co-workers[30]. ^{1}H NMR (200 MHz, DMSO): δ ppm: 8.87 and 8.25 (d, 4H), aromatic group of the diazonium function, 7.5 to 7.8 (m, 5H aromatics) from the commercial 4-aminobenzophenone.

2.3 Raman and SERS measurements

SERS and extinction measurements were recorded using Xplora ONE (Horiba scientific) spectrometer. For SERS, a 660 nm laser tuned at 3 µW was focused on the sample with x80 objective (N.A. 0.75). The used grating of 600 grooves.mm^{-1} ensured a spectral resolution of 3 cm^{-1}. Integration time for signal collection was set at 40s. Each spectrum was the average of two repetitive accumulations. The mean spectra presented here are the average of five spectra acquired on different location of the sample.

2.4 Chemometrics

As mentioned in the introduction, an ICA process was applied to the SERS spectra. This method decomposes a spectrum into linear combination of synthetic spectra called components and their coefficients are called scores. The estimated independent components (ICs) are often closely related to the spectral profiles of the individual chemical components in the initial mixture and thus chemically interpretable[31,32].

Then a Partial least squares-discriminant analysis (PLS-DA) method was applied to analyze SERS spectra in the presence of different drugs. PLS-DA is a technique used for predictive and descriptive modelling as well as for discriminative variable selection. This method aims to maximize the covariance between SERS spectra and the corresponding classes (different drugs) by finding a linear subspace of the variables[33].

To facilitate the comparison among the spectra, the signal was normalized by dividing each spectrum by its Euclidean norm.

All pretreatments and chemometric applications were performed using Matlab software R2017b (The MathWorks, Natick, USA).

2.5 MIP grafting on gold NC

Gold nano-cylinders arrays were elaborated on indium–tin-oxide (ITO) coated-glass substrates by electron-beam lithography (EBL). The functionalization of gold NCs arrays by MIPs was performed using a chemical strategy based on aryl diazonium salt initiators[34–36]. These molecules were chosen as an alternative to alkanethiol self-assembled monolayers, in order to obtain stable and strongly attached layers at the surface of the plasmonic arrays. The grafting process is summarized on Figure 1. A bifunctional initiator, 4-benzoylbenzenediazonium tetrafluoroborate, bearing (i) a diazonium end group for surface anchoring and (ii) a benzophenone function able to activate surface-initiated radical photopolymerization was synthesized according to ref[37]. The NCs were functionalized with the initiator-derived diazonium salts by simple incubation of the arrays in a water solution of the diazonium salt (3 mM) at room temperature for 2 h. After washing the plasmonic arrays with copious amount of water and ethanol, photopolymerization could proceed, incubating the NC arrays with a deoxygenated mixture of MAA (1 mmol) as the monomer, EGDMA (1.5 mmol) as the crosslinking agent, dimethylamine (DMA: 4wt.% relative to MMA and EGDMA)) as co-initiator and paracetamol (0.25 mmol) as the template molecule. Irradiation of the mixture under UV light for 4 h yielded the final products, consisting of NC arrays coated by molecularly imprinted polymers (Au@MIP). A reference non-imprinted polymer sample (Au@NIP) was prepared using the same procedure, but without the addition of the paracetamol template.

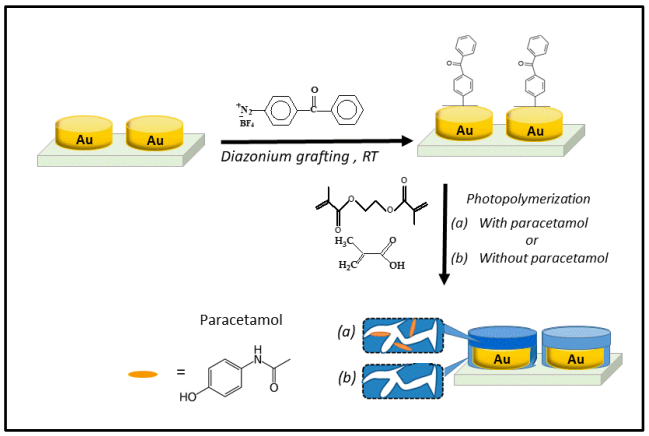

Figure 1. Schematic illustration of the surface modification strategy for coating the gold NC arrays with a MIPs layer, by combining diazonium salt chemistry and photopolymerization.

3 RESULTS AND DISCUSSION

Representative SEM images of the NCs are displayed in figure 2. They exhibit a diameter D = 100 nm, a height H = 50 nm, and an interparticle distance Λ = 200 nm. The extinction spectrum of the NC array shows a main peak at 639 nm, corresponding to the localized surface plasmon resonance (LSPR). The plasmon band shifts to 682 nm after grafting of MIP and to 680 nm after washing the paracetamol from the MIP. This behavior is coherent with an increase of the local refractive index due to the grafting of the organic coating around the gold NCs and then a decrease when the paracetamol is removed. The shift of the LSPR with the paracetamol removal suggest that the layer is thin enough for the surface to be sensitive to chemical modifications. Electromagnetic simulations (can be found here: [38]) confirm that the volume in which the LSPR can detect any change is a few nanometer wide.

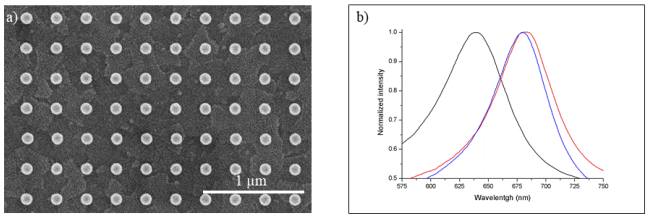

Figure 2. Characterization of the gold NC array. (a) SEM image of the nanoarray with cylinders of 100 nm in diameter and a pitch of 200 nm. (b) Normalized extinction spectra showing the LSP of the NCs: (black) before MIPs functionalization, (red) after functionalization and (blue) after washing the paracetamol.

The surface chemical composition of the NCs after functionalization was investigated by XPS. Only slight modifications of the spectra were observed after the reaction with the diazonium salt-derived initiator, suggesting that the grafted initiator layer is very thin. No peak that could be attributed to nitrogen atoms from the diazonium group can be observed, evidencing the complete transformation of the diazonium cations. In contrast, the polymerization step induces strong variation of the XPS spectra, summarized in Table 1. The most striking observation is the progressive decrease of the gold signal and the relative increase of carbon and nitrogen due to the poly(MAA-co-EGDMA) coating.

Material	**Au**	**C**	**O**	**N**
Au NCs	42	42	13	3
Au@Benzophenone	43	49	6	2
Au@MIP	2	71	21	6
Au@NIP	-	72	22	6

Table 1. Surface chemical composition (at. %) of initial Au NCs, Au@Benzophenone, Au@MIP and Au@NIP.

The samples were further characterized by SERS (see Figure 3). The Raman spectra were successively acquired on the bare NCs, the Au@MIP and the Au@NIP just after grafting and after washing the paracetamol away from the polymer. After washing, the Au@NIP spectra show variations reflecting modifications of the polymer matrix. For instance, the peaks at 1615 cm^{-1} and 1388 cm^{-1} are better defined once the Au@NIP has been rinsed. Similarly, the comparison between the Au@MIP spectra recorded before and after washing, evidences slight modifications. The peaks at 933 cm^{-1}, 1201 cm^{-1}, 1388 cm^{-1} and 1615 cm^{-1} cannot be seen when the paracetamol is in the matrix but appear clearly after washing. These peaks are comparable to those seen in the rinsed Au@NIP and can thus be assigned to the polymer matrix layer. The spectrum of the paracetamol does not emerge. This can be explained by the fact that the vibrational modes of the drug are strongly affected by the polymer matrix. Also, the paracetamol concentration is very likely too low compared to the polymer one. The decrease or disappearance of some of the MIP's peaks (1201 cm^{-1} peak for instance) reveals the growing interaction between the polymer and paracetamol, and thus the presence of the contaminant.

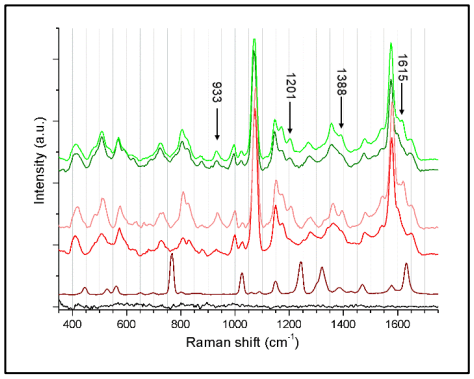

Figure 3. SERS spectra of the bare cylinders (black); Au@MIP before (red) and after (light red) washing away the paracetamol; Au@NIP before (dark green) and after (light green) washing the polymer. The brown curve is the Raman spectra (without NC) of the paracetamol powder.

Increasing concentrations solutions of paracetamol were added to the Au@MIP and Au@NIP samples in order to analyze the evolution of the SERS peaks intensity (Figure 4). As observed above, the paracetamol molecular fingerprint cannot be seen in the Au@MIP spectra. However, some of the peaks of the Au@MIP decrease in intensity as the concentration in paracetamol increases, especially the 2 prominent peaks at 1073 cm^{-1} and 1579 cm^{-1}. The spectra of the Au@NIP show minor variation as the polymer is exposed to increasing concentrations of paracetamol.

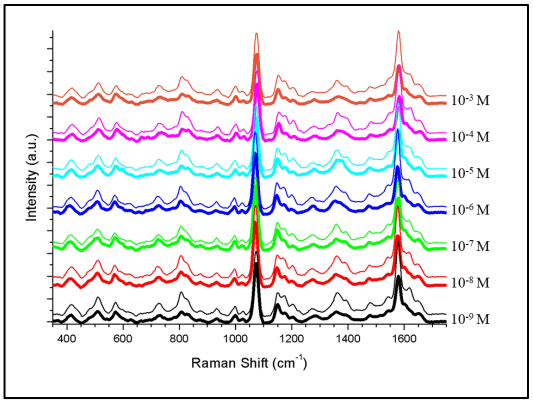

Figure 4. SERS spectra of the MIP (thick lines) and NIP (thin lines) exposed to increasing concentration of paracetamol

From this observation, a calibration curve has been derived and is shown on figure 5. The intensity of the peak at 1073 cm^{-1} (I_{1073}) was plotted for each concentration. As expected, I_{1073} was observed to decrease for Au@MIP with increasing concentration of paracetamol. The experimental points were then fitted to measure the sensitivity of the sensor. The absence of a plateau shows that even at 1 mM, the SERS-MIP sensor is not saturated. The limit of detection (LoD) (i.e. the smallest reasonable value detected) is given by the intersection of the calibration curve and the curve of equation $\langle x_{bl} \rangle + k\,\sigma$, where $\langle x_{bl} \rangle$ is the mean intensity of the blank sample, σ is its standard deviation and k is a parameter reflecting the confidence level of the detection. The LoD of the SERS-MIP sensors is given by the intersection between the green and red curve and it is less than 300 nM (45 $\mu g.l^{-1}$).

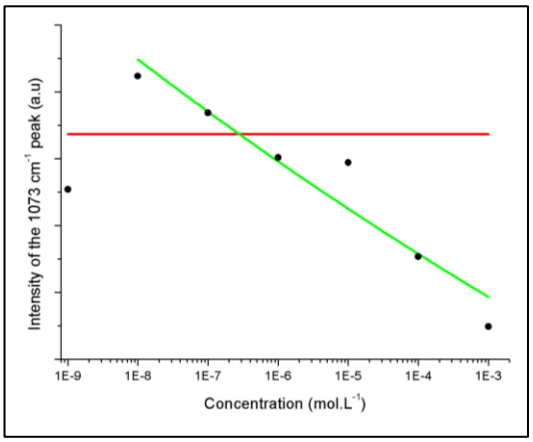

Figure 5. Calibration curve from the intensity of peak 1073 cm^{-1}. Black dot: experimental point and green line fit. Red line: LoD

As paracetamol is an emerging contaminant that has been detected in different environmental water at concentrations ranging from 50 to 80 $\mu g.L^{-1}$,[39] the characteristics of the Au@MIP sensor described here, appear well adapted for detection of paracetamol in real sample concentration ranges.

The SERS analysis described above was further confirmed by means of multivariate analysis. An Independent Component Analysis (ICA) was used on the rough paracetamol spectra. On the top part of Figure 6, each point represents the score of the first component of each spectrum. The Au@MIP (point 1 to 30) have clearly a lower score than the Au@NIP (point 31 to 60). The difference between the two kinds of samples is thus confirmed by the ICA analysis. In order to test the selectivity and the reusability of the sensor, a series of consecutive measurements was made on the same Au@MIP sample. After a first SERS measurement, the sample was washed and measured again. The procedure was repeated with an exposition to salicylic acid and acetylsalicylic acid (two molecules with similar structures to paracetamol). The result of the PLS-DA analysis is shown on the bottom part of figure 6. The score obtained for the rinsed sample is clearly higher than those obtained in presence of a drug. The red dot line of figure 6 is the calculated discrimination of the empty MIP. The score obtained for the salicylic and acetylsalicylic acids are of the same order while the score of paracetamol is lower, confirming the selectivity of the nanosensor towards paracetamol.

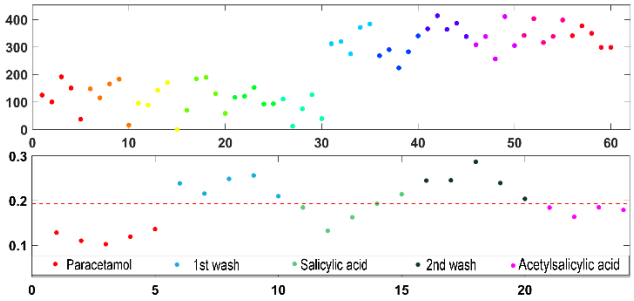

Figure 6. ICA analysis of the SERS spectra. Each point represents a spectrum. Up: the first component of the analysis makes a good separation between the MIP (point 1 to 30) and the NIP (point 31 to 60). Bottom: the analysis of the same samples in the presence of different drugs using PLS-DA. The red dot line shows the discrimination between the paracetamol and the other state of the polymer

4 CONCLUSION

In conclusion, we have designed and produced a hybrid sensor made from the grafting of a MIP on gold nanocylinders. This sensor was able to detect paracetamol in water with a limit of detection of 300 nM. It also presents a good sensitivity and selectivity. The sensor has demonstrated a good reproducibility and specificity. The use of multivariate analysis confirmed the results obtained by classical analysis. The results presented here are a proof of concept that the detection of emerging pollutants such as paracetamol is possible in a routine way. Other results have demonstrated that it was possible to take advantage of the polarization of the light to perform a regio-selective functionalization of the nanocylinders [40]. These complementary results pave the way to ultra-sensitive multiplexed SERS sensors.

ACKNOWLEDGEMENTS

The authors would like to thanks the C'Nano for its financial support in the framework of the SYRENSS project.

REFERENCES

[1] M.J. Whitcombe, I. Chianella, L. Larcombe, S.A. Piletsky, J. Noble, R. Porter, A. Horgan, The rational development of molecularly imprinted polymer-based sensors for protein detection, Chem. Soc. Rev. (2011). doi:10.1039/c0cs00049c.

[2] J.J. BelBruno, Molecularly Imprinted Polymers, Chem. Rev. 119 (2019) 94–119. doi:10.1021/acs.chemrev.8b00171.

[3] R. Ahmad, N. Félidj, L. Boubekeur-Lecaque, S. Lau-Truong, S. Gam-Derouich, P. Decorse, A. Lamouri, C. Mangeney, Water-soluble plasmonic nanosensors with synthetic receptors for label-free detection of folic acid, Chem. Commun. 51 (2015)

9678–9681. doi:10.1039/C5CC01489A.
[4] K. Haupt, K. Mosbach, Molecularly Imprinted Polymers and Their Use in Biomimetic Sensors, Chem. Rev. 100 (2000) 2495–2504. doi:10.1021/cr990099w.
[5] A. Rico-Yuste, S. Carrasco, Molecularly imprinted polymer-based hybrid materials for the development of optical sensors, Polymers (Basel). 11 (2019). doi:10.3390/polym11071173.
[6] G. Vasapollo, R. Del Sole, L. Mergola, M.R. Lazzoi, A. Scardino, S. Scorrano, G. Mele, Molecularly Imprinted Polymers: Present and Future Prospective, Int. J. Mol. Sci. 12 (2011) 5908–5945. doi:10.3390/ijms12095908.
[7] L. a. Dick, A.D. McFarland, C.L. Haynes, R.P. Van Duyne, Metal film over nanosphere (MFON) electrodes for surface-enhanced Raman spectroscopy (SERS): Improvements in surface nanostructure stability and suppression of irreversible loss, J. Phys. Chem. B. 106 (2002) 853–860. doi:10.1021/jp013638l.
[8] M. Cottat, C. D'Andrea, R. Yasukuni, N. Malashikhina, R. Grinyte, N. Lidgi-Guigui, B. Fazio, A. Sutton, O. Oudar, N. Charnaux, V. Pavlov, A. Toma, E. Di Fabrizio, P.G. Gucciardi, M. Lamy de la Chapelle, High Sensitivity, High Selectivity SERS Detection of MnSOD Using Optical Nanoantennas Functionalized with Aptamers, J. Phys. Chem. C. 119 (2015) 15532–15540. doi:10.1021/acs.jpcc.5b03681.
[9] I. Tijunelyte, S. Betelu, J. Moreau, I. Ignatiadis, C. Berho, N. Lidgi-Guigui, E. Guénin, C. David, S. Vergnole, E. Rinnert, M.L. De La Chapelle, Diazonium salt-based surface-enhanced Raman spectroscopy nanosensor: Detection and quantitation of aromatic hydrocarbons in water samples, Sensors (Switzerland). 17 (2017). doi:10.3390/s17061198.
[10] T. Schmid, L. Opilik, C. Blum, R. Zenobi, Nanoscale Chemical Imaging Using Tip-Enhanced Raman Spectroscopy: A Critical Review, Angew. Chemie Int. Ed. 52 (2013) 5940–5954. doi:10.1002/anie.201203849.
[11] X. Qian, X.-H. Peng, D.O. Ansari, Q. Yin-Goen, G.Z. Chen, D.M. Shin, L. Yang, A.N. Young, M.D. Wang, S. Nie, In vivo tumor targeting and spectroscopic detection with surface-enhanced Raman nanoparticle tags., Nat. Biotechnol. 26 (2008) 83–90. doi:10.1038/nbt1377.
[12] W. Zhang, B.S. Yeo, T. Schmid, R. Zenobi, Single Molecule Tip-Enhanced Raman Spectroscopy with Silver Tips, J. Phys. Chem. C. 111 (2007) 1733–1738. doi:10.1021/jp064740r.
[13] S. Nie, Probing Single Molecules and Single Nanoparticles by Surface-Enhanced Raman Scattering, Science (80-.). 275 (1997) 1102–1106. doi:10.1126/science.275.5303.1102.
[14] C. Delhaye, J.L. Bruneel, D. Talaga, M. Guirardel, S. Lecomte, L. Servant, Tailoring surface-enhanced Raman scattering effect using microfluidics, J. Phys. Chem. C. 116 (2012) 5327–5332. doi:10.1021/jp209169r.
[15] F. Járai-Szabó, S. Aştilean, Z. Néda, Understanding self-assembled nanosphere patterns, Chem. Phys. Lett. 408 (2005) 241–246. doi:10.1016/j.cplett.2005.04.051.
[16] C. Farcau, S. Astilean, Mapping the SERS Efficiency and Hot-Spots Localization on Gold Film over Nanospheres Substrates, J. Phys. Chem. C. 114 (2010) 11717–11722. doi:10.1021/jp100861w.
[17] M. Cottat, N. Lidgi-Guigui, I. Tijunelyte, G. Barbillon, F. Hamouda, P. Gogol, A. Aassime, J.-M. Lourtioz, B. Bartenlian, M.L. de la Chapelle, Soft UV nanoimprint lithography-designed highly sensitive substrates for SERS detection, Nanoscale Res. Lett. 9 (2014). doi:10.1186/1556-276X-9-623.
[18] * Zhong-Qun Tian, and Bin Ren, D.-Y. Wu, Surface-Enhanced Raman Scattering: From Noble to Transition Metals and from Rough Surfaces to Ordered Nanostructures, (2002). doi:10.1021/JP0257449.
[19] X. Zhao, J. Dong, E. Cao, Q. Han, W. Gao, Y. Wang, J. Qi, M. Sun, Plasmon-exciton coupling by hybrids between graphene and gold nanorods vertical array for sensor, Appl. Mater. Today. 14 (2019) 166–174. doi:10.1016/j.apmt.2018.12.013.
[20] A.E. Cetin, C. Yilmaz, B.C. Galarreta, G. Yilmaz, H. Altug, A. Busnaina, Fabrication of Sub-10-nm Plasmonic Gaps for Ultra-Sensitive Raman Spectroscopy, Plasmonics. (2020) 1–7. doi:10.1007/s11468-020-01137-3.
[21] R.A. Tripp, R.A. Dluhy, Y. Zhao, Novel nanostructures for SERS biosensing, Nano Today. 3 (2008) 31–37. doi:10.1016/S1748-0132(08)70042-2.
[22] M. Dribek, E. Rinnert, F. Colas, M.-P. Crassous, N. Thioune, C. David, M. de la Chapelle, C. Compère, Organometallic nanoprobe to enhance optical response on the polycyclic aromatic hydrocarbon benzo[a]pyrene immunoassay using SERS technology, Environ. Sci. Pollut. Res. 24 (2017) 27070–27076. doi:10.1007/s11356-014-3384-8.
[23] J.B. Schlenoff, M. Li, H. Ly, Stability and Self-Exchange in Alkanethiol Monolayers, J. Am. Chem. Soc. 117 (1995) 12528–12536. doi:10.1021/ja00155a016.
[24] † Xingyu Jiang, † Rosaria Ferrigno, ‡ and Milan Mrksich, † George M. Whitesides*, Electrochemical Desorption of Self-Assembled Monolayers Noninvasively Releases Patterned Cells from Geometrical Confinements, (2003). doi:10.1021/JA029485C.
[25] B. Kasprzyk-Hordern, R.M. Dinsdale, A.J. Guwy, The occurrence of pharmaceuticals, personal care products, endocrine disruptors and illicit drugs in surface water in South Wales, UK, Water Res. 42 (2008) 3498–3518. doi:10.1016/j.watres.2008.04.026.
[26] C.I. Kosma, D.A. Lambropoulou, T.A. Albanis, Investigation of PPCPs in wastewater treatment plants in Greece: Occurrence, removal and environmental risk assessment, Sci. Total Environ. 466–467 (2014) 421–438. doi:10.1016/J.SCITOTENV.2013.07.044.
[27] I. González-Mariño, E. Gracia-Lor, N.I. Rousis, E. Castrignanò, K. V. Thomas, J.B. Quintana, B. Kasprzyk-Hordern, E. Zuccato, S. Castiglioni, Wastewater-Based Epidemiology To Monitor Synthetic Cathinones Use in Different European Countries, Environ. Sci. Technol. 50 (2016) 10089–10096. doi:10.1021/acs.est.6b02644.
[28] I. González-Mariño, R. Rodil, I. Barrio, R. Cela, J.B. Quintana, Wastewater-Based Epidemiology as a New Tool for Estimating Population Exposure to Phthalate Plasticizers, Environ. Sci. Technol. 51 (2017) 3902–3910. doi:10.1021/acs.est.6b05612.
[29] M. Bedner, W.A. MacCrehan, Transformation of acetaminophen by chlorination produces the toxicants 1,4-benzoquinone and N-acetyl-p-benzoquinone imine, Environ. Sci. Technol. 40 (2006) 516–522. doi:10.1021/es0509073.
[30] 1d Philippe Allongue, 1b Michel Delamar, 1c Bernard Desbat, 1a Olivier Fagebaume, 1a Rachid Hitmi, *,1a and Jean Pinson, 1a Jean-Michel Savéant*, Covalent Modification of Carbon Surfaces by Aryl Radicals Generated from the Electrochemical Reduction of Diazonium Salts, (1997). doi:10.1021/JA963354S.
[31] A. Hyvärinen, E. Oja, Independent component analysis: algorithms and applications., Neural Netw. 13 (n.d.) 411–30. http://www.ncbi.nlm.nih.gov/pubmed/10946390 (accessed June 12, 2019).
[32] D.N. Rutledge, D. Jouan-Rimbaud Bouveresse, Independent Components Analysis with the JADE algorithm, TrAC Trends Anal. Chem. 50 (2013) 22–32. doi:10.1016/J.TRAC.2013.03.013.
[33] R.G. Brereton, G.R. Lloyd, Partial least squares discriminant analysis: taking the magic away, J. Chemom. 28 (2014) 213–225. doi:10.1002/cem.2609.
[34] M. Nguyen, X. Sun, E. Lacaze, P.M. Winkler, A. Hohenau, J.R. Krenn, C. Bourdillon, A. Lamouri, J. Grand, G. Lévi, L. Boubekeur-Lecaque, C. Mangeney, N. Félidj, Engineering Thermoswitchable Lithographic Hybrid Gold Nanorods as Plasmonic Devices for Sensing and Active Plasmonics Applications, ACS Photonics. 2 (2015) 1199–1208. doi:10.1021/acsphotonics.5b00280.
[35] M. Nguyen, N. Felidj, C. Mangeney, Looking for Synergies in Molecular Plasmonics through Hybrid Thermoresponsive Nanostructures, Chem. Mater. 28 (2016) 3564–3577. doi:10.1021/acs.chemmater.6b00230.
[36] R. Ahmad, L. Boubekeur-Lecaque, M. Nguyen, S. Lau-Truong, A. Lamouri, P. Decorse, A. Galtayries, J. Pinson, N. Felidj, C. Mangeney, Tailoring the Surface Chemistry of Gold Nanorods through Au–C/Ag–C Covalent Bonds Using Aryl Diazonium Salts, J. Phys. Chem. C. 118 (2014) 19098–19105. doi:10.1021/jp504040d.
[37] S. Gam-Derouich, B. Carbonnier, M. Turmine, P. Lang, M. Jouini, D. Ben Hassen-Chehimi, M. M. Chehimi, Electrografted Aryl Diazonium Initiators for Surface-Confined

Photopolymerization: A New Approach to Designing Functional Polymer Coatings, Langmuir. 26 (2010) 11830–11840. doi:10.1021/la100880j.

[38] F. Colas, D. Barchiesi, S. Kessentini, T. Toury, M.L. de la Chapelle, Comparison of adhesion layers of gold on silicate glasses for SERS detection, J. Opt. 17 (2015) 114010. doi:10.1088/2040-8978/17/11/114010.

[39] J. Żur, A. Piński, A. Marchlewicz, K. Hupert-Kocurek, D. Wojcieszyńska, U. Guzik, Organic micropollutants paracetamol and ibuprofen—toxicity, biodegradation, and genetic background of their utilization by bacteria, Environ. Sci. Pollut. Res. 25 (2018) 21498–21524. doi:10.1007/s11356-018-2517-x.

[40] I. Tijunelyte, I. Kherbouche, S. Gam-Derouich, M. Nguyen, N. Lidgi-Guigui, M.L. De La Chapelle, A. Lamouri, G. Lévi, J. Aubard, A. Chevillot-Biraud, C. Mangeney, N. Felidj, Multi-functionalization of lithographically designed gold nanodisks by plasmon-mediated reduction of aryl diazonium salts, Nanoscale Horizons. 3 (2018). doi:10.1039/c7nh00113d.

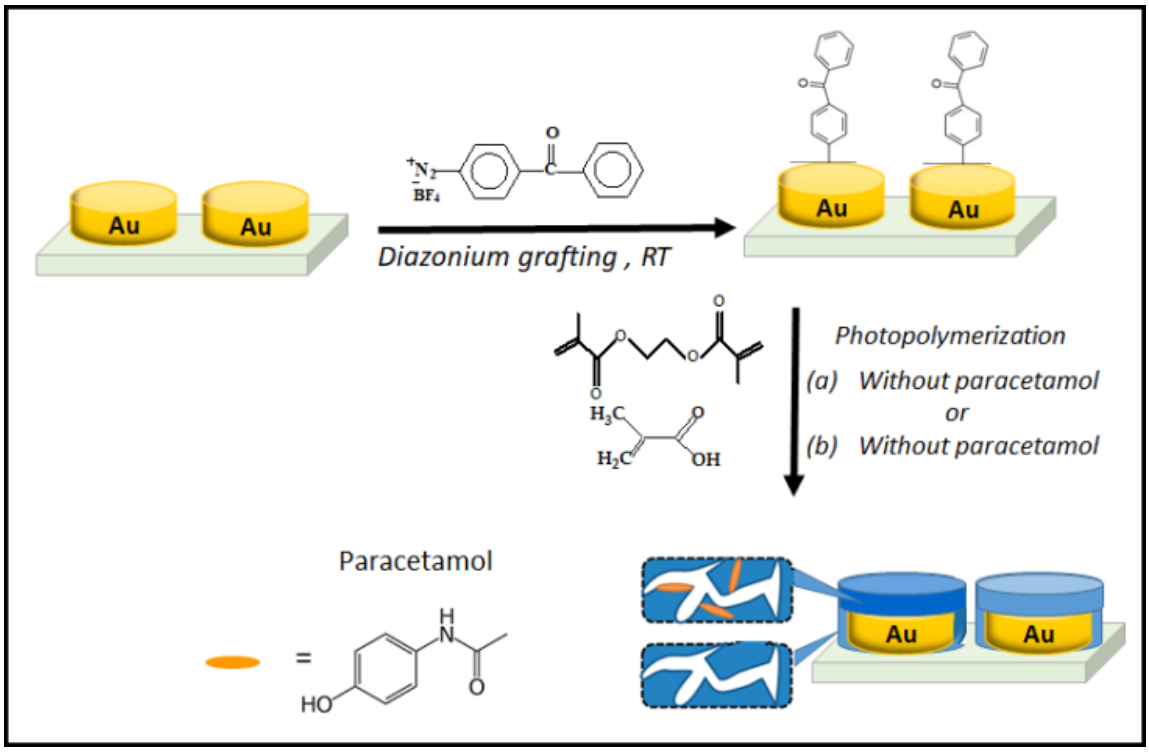

Figure 1. Schematic illustration of the surface modification strategy for coating the gold NC arrays with a MIP layer, by combining diazonium salt chemistry and photopolymerization.

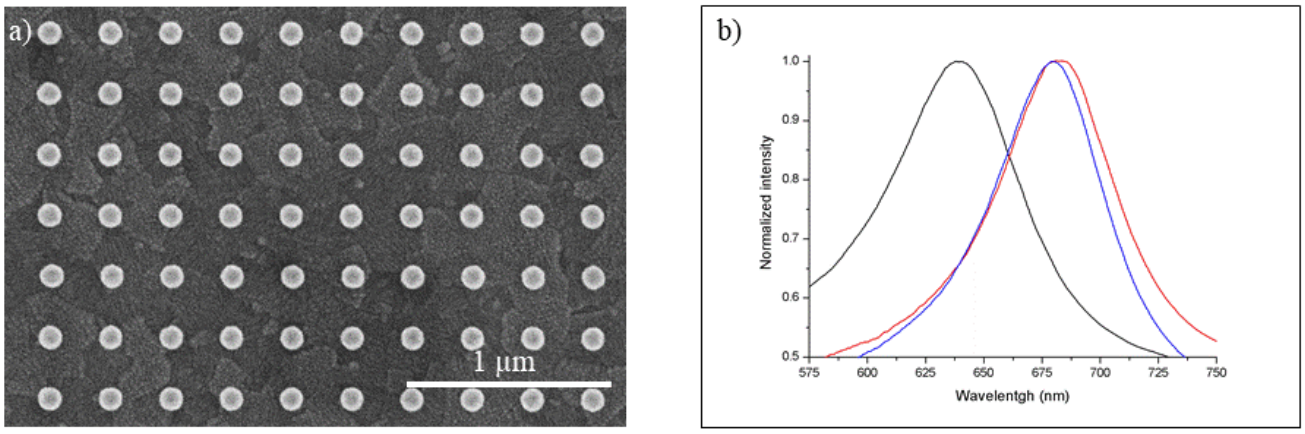

Figure 2. Characterization of the gold NCs array. (a) SEM image of the nanoarray with disks of 100 nm in diameter and a pitch of 200 nm. (b) Extinction spectra showing the LSP of the NCs: (black) before MIP functionalization, (red) after functionalization and (blue) after washing the paracetamol.

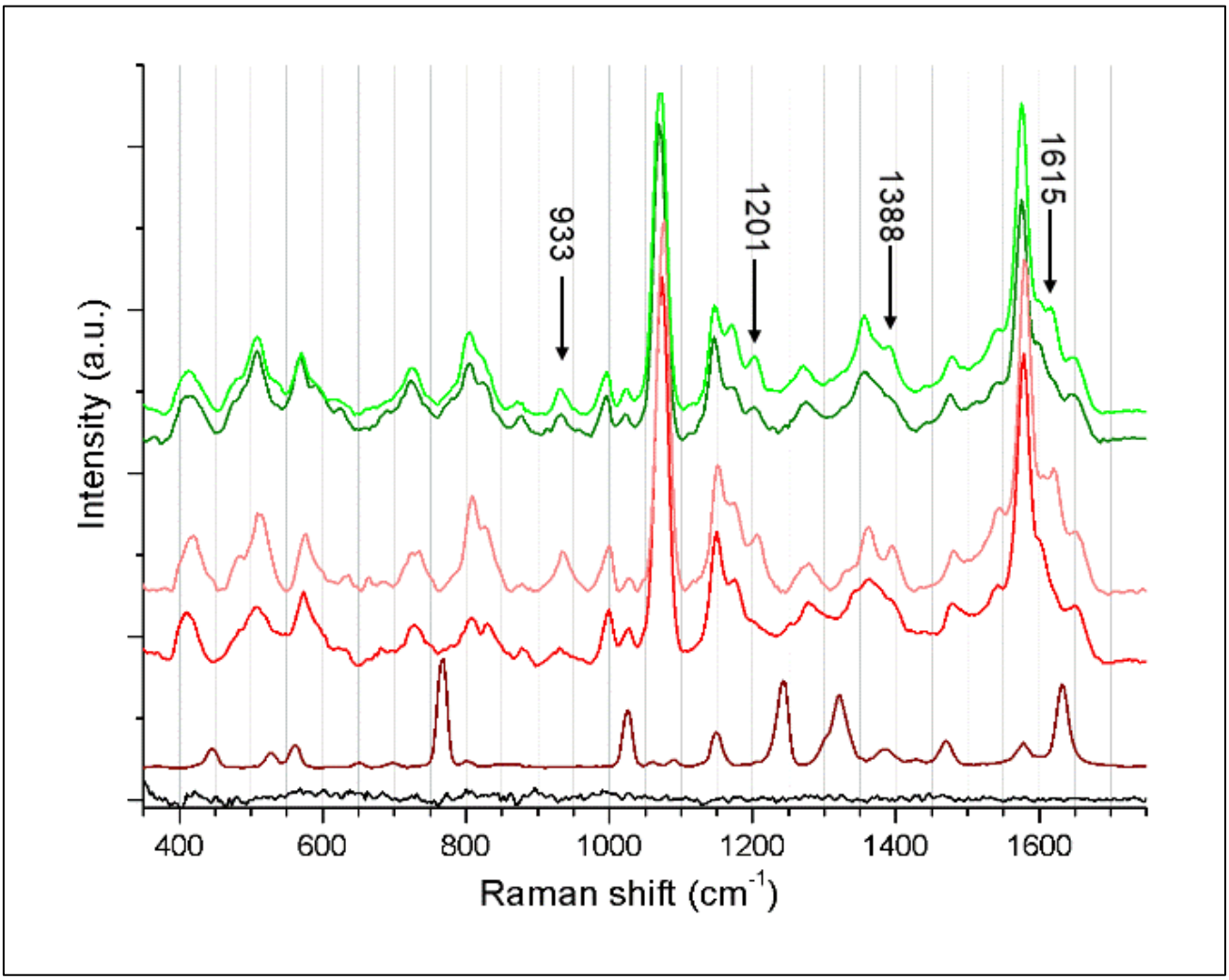

Figure 3. SERS spectra of the bare cylinders (black); Au@MIP before (red) and after (light red) washing away the paracetamol; Au@NIP before (dark green) and after (light green) washing the polymer. The brown curve is the Raman spectra (without NC) of the paracetamol powder.

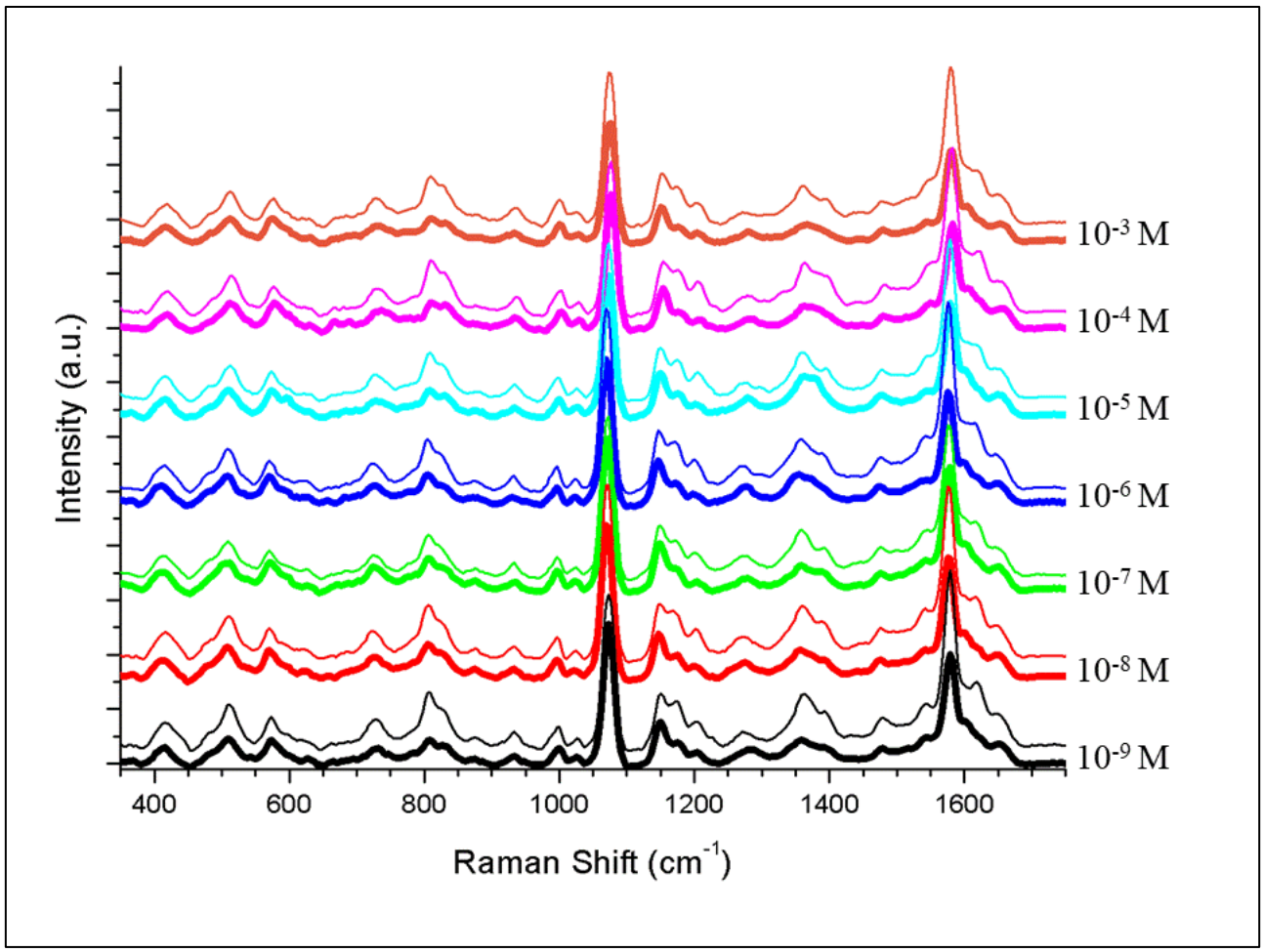

Figure 4. SERS spectra of the MIP (thick lines) and NIP (thin lines) exposed to increasing concentration of paracetamol

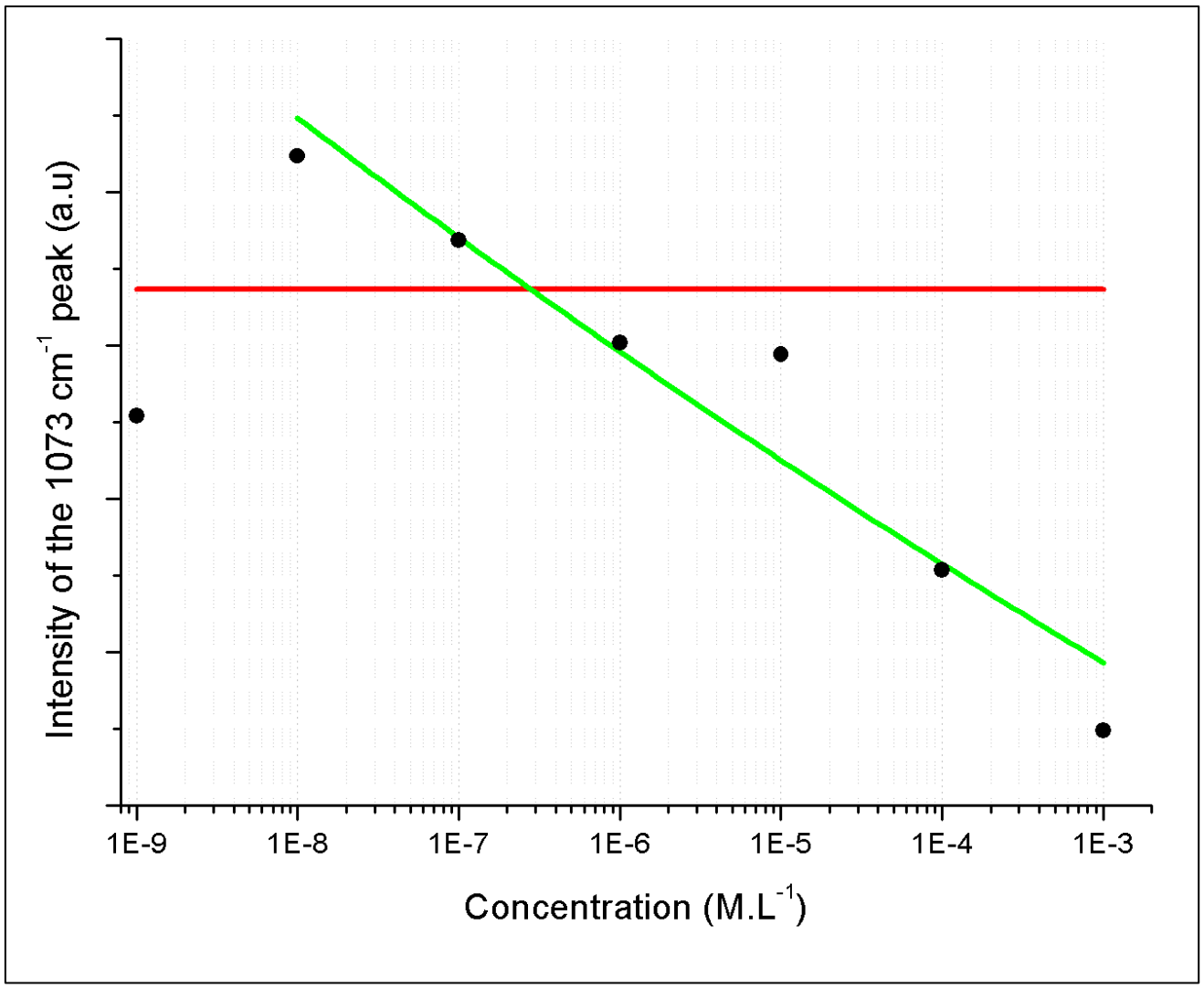

Figure 5. Calibration curve from the intensity of peak 1073 cm^{-1}. Black dot: experimental point and green line fit. Red line: LoD

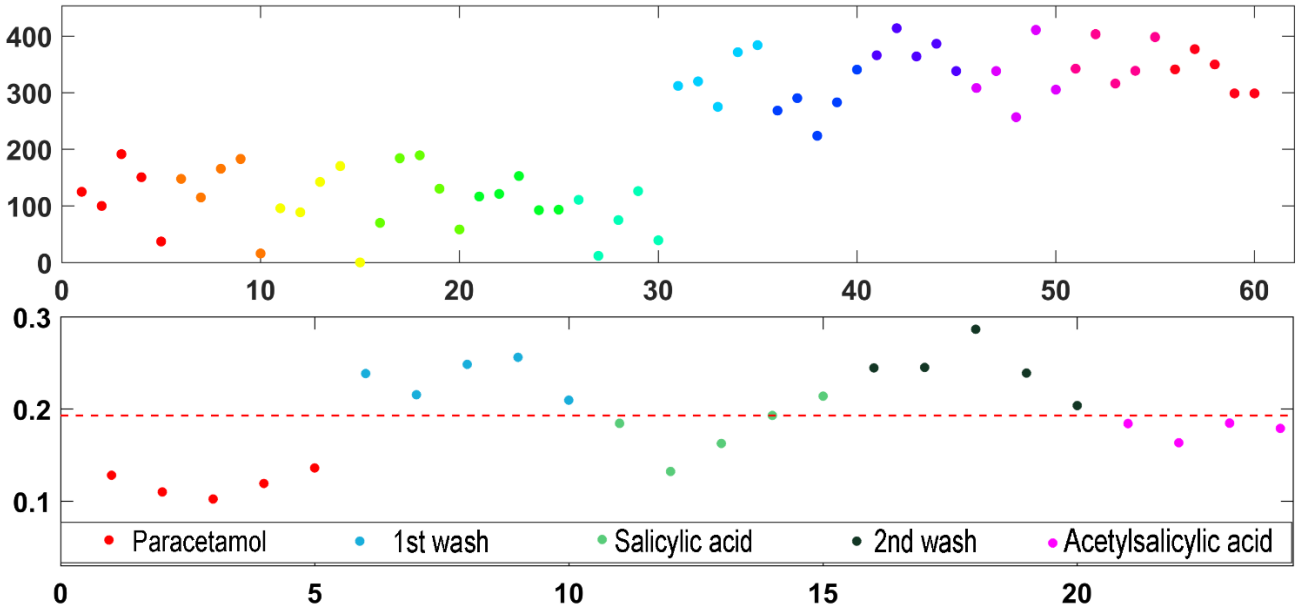

Figure 6. ICA analysis of the SERS spectra. Each point represents a spectrum. Up: the first component of the analysis makes a good separation between the MIP (point 1 to 30) and the NIP (point 31 to 60). Bottom: the analysis of the same samples in the presence of different drugs using PLS-DA. The red dot line shows the discrimination between the paracetamol and the other state of the polymer